

## Magnetic memory in ferromagnetic thin films via exchange coupling

K. Chesnel,<sup>1,\*</sup> E. E. Fullerton,<sup>2,†</sup> M. J. Carey,<sup>2</sup> J. B. Kortright,<sup>1</sup> and S. D. Kevan<sup>3</sup><sup>1</sup>Lawrence Berkeley National Laboratory, Berkeley, California 94720, USA<sup>2</sup>Hitachi Global Storage Technologies, San Jose, California 95135, USA<sup>3</sup>Department of Physics, University of Oregon, Eugene, Oregon 97403, USA

(Received 4 June 2008; published 21 October 2008)

We show the possibility of creating magnetic domain memory in thin ferromagnetic films by inducing spatially varying exchange coupling interactions. We evidence this phenomenon in a perpendicular exchange bias film made of [Co/Pd] IrMn multilayers. Our coherent x-ray magnetic scattering speckle correlation study shows that the film exhibits no memory at room temperature but acquires a very high degree of magnetic memory, above 80% with subsequent field cycling when the sample is zero-field cooled below the blocking temperature of the IrMn layers ( $T < 275$  K).

DOI: 10.1103/PhysRevB.78.132409

PACS number(s): 75.70.-i, 42.30.Ms, 75.25.+z

Magnetic memory, the ability of a magnetic system to reproduce its topological domain configuration throughout subsequent magnetization cycles, offers strong potential for technological applications in magnetoelectronics,<sup>1</sup> recording media,<sup>2</sup> and magnetoresistive random access memory (MRAM) devices.<sup>3</sup> Thin ferromagnetic films with perpendicular anisotropy provide an excellent support for these applications, as they form stripe domain patterns.<sup>4</sup> If the film is rough enough, some magnetic memory can be induced in a limited region of the magnetization cycle when magnetic domains nucleate due to the presence of structural defects.<sup>5</sup> However, structural disorder is difficult to control and induces only partial memory. Here we show the possibility of generating magnetic memory without structural defects. In this approach, we use exchange bias (EB) materials to create a well-defined landscape and control very precisely the reversal of the ferromagnetic domains throughout the entire magnetization cycle. In this approach, a ferromagnetic material exhibiting absolutely no intrinsic magnetic memory can acquire a very high degree of magnetic memory on an extended range of magnetic field simply by inducing exchange coupling (EC) interactions with a template imprinted in the antiferromagnetic sublayer.

EC interactions occur when a ferromagnetic (F) material is placed in contact with an antiferromagnetic (AF) material.<sup>6</sup> The EC phenomenon has been extensively exploited in F/AF bilayers with in-plane magnetization<sup>7</sup> and more recently in multilayers with perpendicular anisotropy.<sup>8</sup> The bias effect is due to uncompensated pinned magnetic moments in the AF layer.<sup>9</sup> Most knowledge of EC is based on macroscopic observations, using magnetometry<sup>10</sup> as well as x-ray magnetic circular dichroism.<sup>11</sup> Recent pioneering X-ray scattering,<sup>12–14</sup> magnetic force microscopy,<sup>15</sup> and photoelectron emission microscopy<sup>16–18</sup> studies have evidenced F and AF domains in EB films, stimulating further investigation of the microscopic domain topology and reversal behavior. We use here coherent x-ray scattering measurements to demonstrate memory effects as a direct consequence of exchange couplings.

The experimental system is based on the well-studied Co/Pd multilayers with perpendicular magnetic anisotropy<sup>8</sup> that are periodically interleaved with AF IrMn layers to bias the layers, as sketched in the inset of Fig. 1. Several param-

eters such as the layer thicknesses and stacking order were optimized in order to obtain perpendicular magnetic anisotropy and tune the AF blocking temperature. In the thin-film limit, it is generally found that the exchange bias blocking temperature varies linearly with the AF film thickness.<sup>19</sup> We adjusted the IrMn thickness to achieve a blocking temperature near room temperature (RT) ( $T_B \sim 275$  K), thus resulting in a stack of four repeats of (F) [Co(4 Å)/Pd(7 Å)]<sub>12</sub> multilayers separated by 24 Å of (AF) IrMn alloy. Figure 1 shows the magnetization loops measured by superconducting quantum interference device (SQUID) in two selected conditions: above  $T_B$  at 300 K and below  $T_B$  at 8 K in the zero-field-cooled (ZFC) state, obtained by cooling the film after demagnetizing it to point A. The room-temperature loop shows the features of perpendicular films with a remnant magnetic stripe domain state. Unlike in field-cooled conditions, the ZFC magnetization loop exhibits no macroscopic

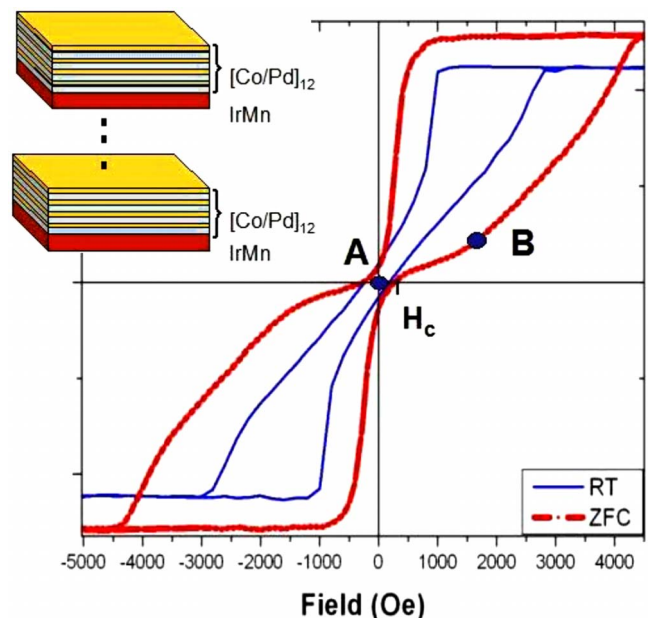


FIG. 1. (Color online) SQUID measurement performed at 300 K (RT) and at 8 K in ZFC state. Inset: sketch of the [Co/Pd]IrMn multilayer.

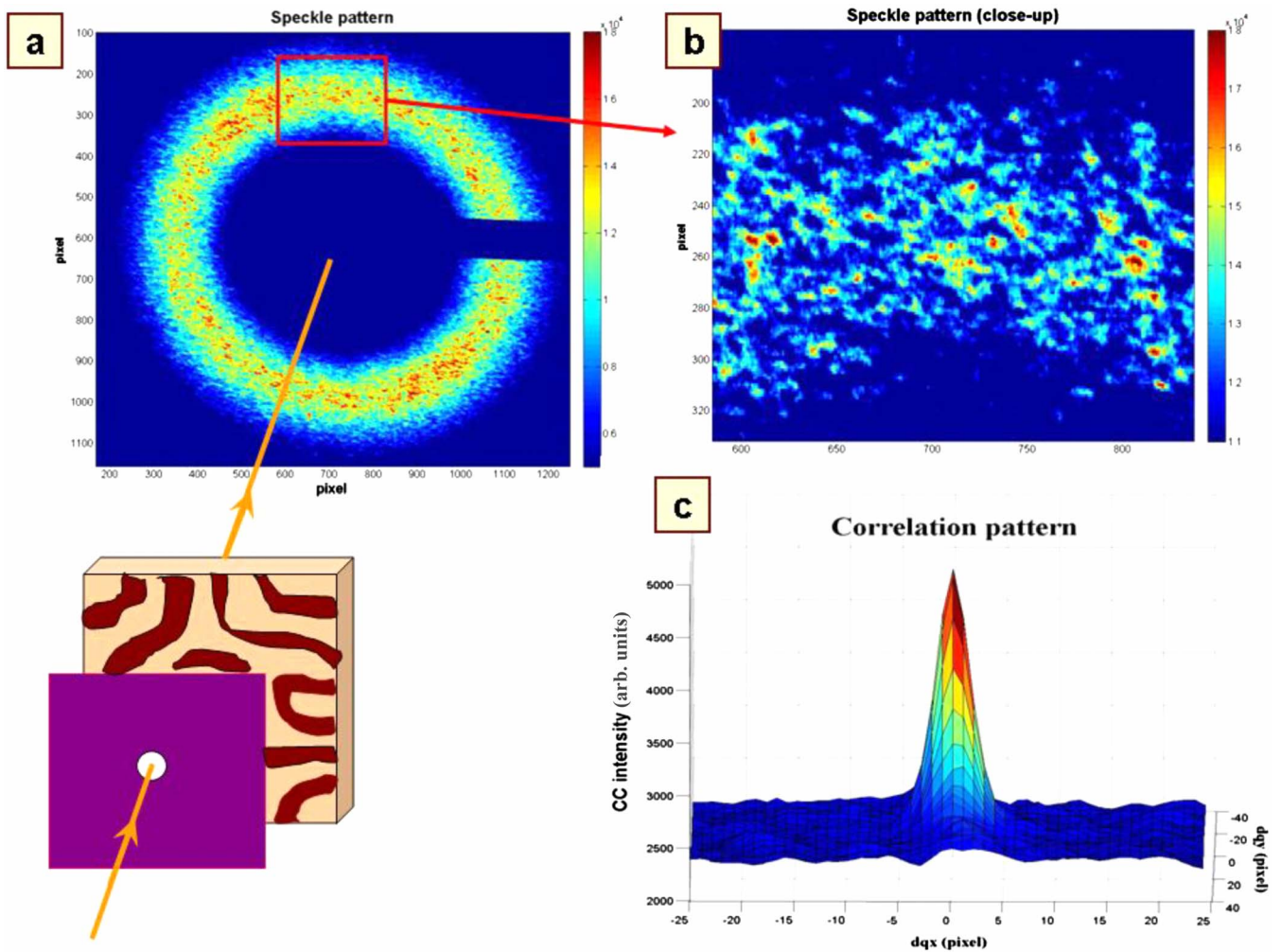


FIG. 2. (Color online) (a) Sketch of the coherent scattering experiment performed in transmission geometry: the sample is mounted perpendicularly to the incident beam in the near field of a 20  $\mu\text{m}$  pinhole fabricated by focused ion-beam etching. Speckle patterns are collected with a CCD detector. The CCD image shown here is measured at the  $\text{Co } L_3$  edge, in ZFC state, at point B of the magnetization loop (Fig. 1). (b) Enlargement of the speckle pattern showing an excellent contrast. (c) RPM cross-correlation pattern obtained from pattern (b). The central peak contains the pure coherent part of the cross-correlated signal from which the degree of magnetic memory is calculated.

bias and remains symmetrical; however its global shape changes significantly from the room-temperature loop. The loop indicates characteristically the presence of bifurcated regions in the film that are either positively or negatively biased.<sup>20,21</sup> The saturation field increases and a plateau appears above the coercive point  $H_c$ , suggesting the existence of a particular favorable magnetic configuration stabilizing the F layer.

Combining the magnetic sensitivity offered by x-ray resonant magnetic scattering (XRMS)<sup>22–24</sup> with the coherence of the light, the technique of *coherent* XRMS gives access to the *local* magnetic topology<sup>25,26</sup> and to reversal processes with *in situ* magnetic field.<sup>27</sup> Under coherent illumination, the light scattered off the sample heterogeneities produces intensity variations known as speckles. While the scattering pattern envelope is related to the ensemble-averaged magnetic order, the specific speckle distribution contains complete information about the local domain topology.<sup>28</sup> We adopt here a cross-correlation (CC) approach<sup>29</sup> to investigate the statistical behavior of the magnetic topology and mag-

netic memory effects. The measurements were performed at the Advanced Light Source, with an instrumentation optimized for coherent soft x rays, offering excellent combination of brightness, temporal, and spatial coherences.<sup>30</sup> A 20  $\mu\text{m}$  circular pinhole is used as a spatial filter to enhance transverse coherence. The scattering experiment is performed in transmission geometry, as shown on Fig. 2(a). The photon energy is tuned to the  $\text{Co } L_3$  edge to enhance the magneto-optical contrast.<sup>22</sup> The use of linear polarization eliminates magnetic-charge interference, leaving only pure magnetic scattering from domains as the sole magnetic contribution in these measurements.<sup>31</sup>

Speckle patterns were recorded along the magnetization loop above and below  $T_B$ . Figure 2(a) shows a charge-coupled device (CCD) image collected in the ZFC state. At nucleation, the scattering pattern has a disk shape, which gradually transforms into a ring shape, thus reflecting formation of labyrinth stripe domains. The radius of the ring indicates that the magnetic period progressively decreases as the reversal progresses to reach a minimum value of 320 nm

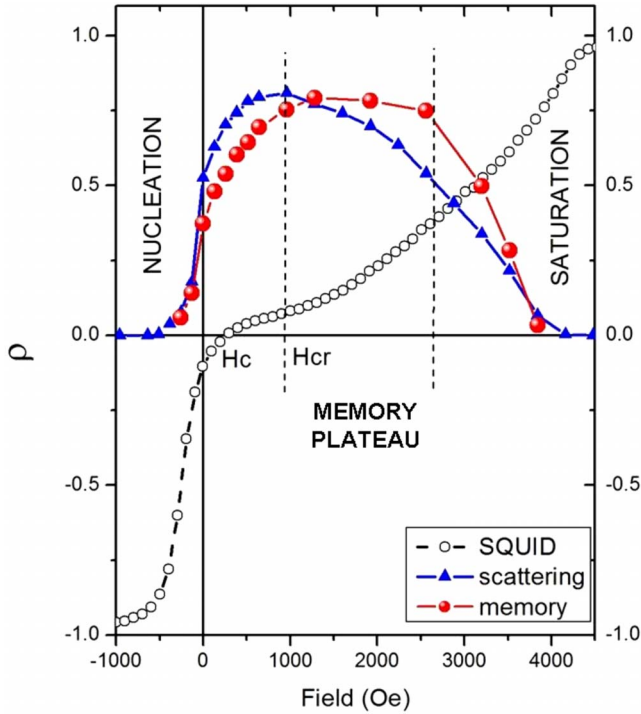


FIG. 3. (Color online) RPM coefficient  $\rho$  (plain dots) as a function of field along the ascending magnetization branch. Each point results from the average of six successive measures. The ascending branch of the SQUID measurement (circles) and scattering intensity (triangles) are plotted together with the memory  $\rho$  after normalization for comparison purposes.

with a correlation length of  $\sim 1 \mu\text{m}$ . Figure 3 (triangle) shows the scattering intensity integrated over the whole image and normalized for comparison purposes, as a function of magnetic field through the ascending branch of the magnetization loop. Starting from the nucleation point, the intensity increases to reach a maximum near the coercive point where half of the domains are reversed, and further decreases to vanish at saturation. The nucleation (disk phase) occurs very sharply and quickly leads to periodic stripe domains (ring phase), which remain present but smoothly vanish toward saturation. Further information about local magnetic topology is provided by the coherent speckle features in these images. Figure 2(b) shows an enlargement of the scattering pattern (a) emphasizing the high speckle contrast, which gives excellent sensitivity for the correlation studies discussed below.

Memory of the magnetic domain topology is quantified by correlating speckle patterns recorded at specific points along the magnetization loop. We concentrate here on return-point memory (RPM) by correlating patterns taken at the exact same point after complete field cycling. An example of CC function is shown in Fig. 2(c). By integrating the coherent part contained in the central peak and normalizing with similar integrations of both autocorrelation functions, one obtains a correlation coefficient  $\rho$  that reaches the limits of zero if the two speckle patterns are completely distinct and one if they are identical. We therefore quantify the degree of RPM by directly using the number rho. We observe that the material does not show any memory ( $\rho \sim 0$ ) at room temperature

for any field value but remarkably the ZFC state produces a very high RPM ( $\rho \sim 0.8$ ). This reveals how the F layer behavior is modified by the EC interactions with the AF layer. Above  $T_B$ , domain nucleation and propagation occur randomly and not reproducibly. In ZFC condition, the same F layer exhibits a strong magnetic memory by reproducing a particular topological configuration in which the film was cooled. This phenomenon indicates the existence of a magnetic pattern in the AF layer, formed by uncompensated spins at the vicinity of the interface with F layer, which plays the role of reference template. This pattern results from the organization of pinned uncompensated Mn moments in the IrMn sublayers. In such configuration, the net magnetization is zero; therefore the film exhibits no macroscopic EB. Nevertheless, there are strong local EC interactions between the F and AF pinned moments at the microscopic level. While the imprinted AF template remains unchanged, the F layer tends to retrieve the same mesoscopic topology after each cycling.

We investigated the global behavior of the magnetic memory through the whole magnetization cycle. Figure 3 (red curve, plain dots) shows the resulting RPM versus magnetic field. The memory is found to be low at the nucleation point and increases sharply as reversal occurs to reach a maximum beyond the coercive point  $H_c$ . This correlation coefficient stays high over an extended field range from 1000 to 2500 Oe, defining a “memory plateau,” and then eventually decreases to zero near saturation.

Importantly, this behavior is fundamentally different from disorder-induced memory<sup>32</sup> where the memory shape is asymmetric with a sharp peak near nucleation followed by a monotonic decline with increasing field strength. The memory plateau shape observed here suggests that domains nucleate in sparse locations that are not pinned by any defects, consistent with smooth films free from microstructural defects such as grain boundaries. Nevertheless, because of the EC interactions, the domains are able to form and grow, adjusting to the underlying AF pattern following an increasingly deterministic path, and eventually reach a high memory, as illustrated by the schematic in Fig. 4. At this memory plateau, half of the domains are reversed and closely reproduce the topology of the frozen AF template.

Another remarkable point is that the RPM does not reach its maximum value right at  $H_c$  (300 Oe) but above  $H_c$ , around 1000 Oe. We associate this point to the remanent coercivity  $H_{cr}$ . Remanent hysteresis loops are measured by first saturating in a negative field and then measuring the remanent magnetization after applying increasingly positive fields. The remanent coercivity  $H_{cr}$  is the positive field that results in the remanent magnetization being zero. This corresponds to the field value necessary to irreversibly reverse half of the magnetization. At  $H_{cr}$ , the system has a net magnetization but only half the spins have effectively flipped irreversibly. When the field is released from  $H_{cr}$  back to zero, the system returns back to a state where the up and down spins are compensated; thus the net magnetization is zero. This suggests that the main contribution to magnetic memory is given by the magnetic domains that have flipped irreversibly, leaving some degree of freedom for reversible domain-wall motion. In the memory plateau, the reversal progresses

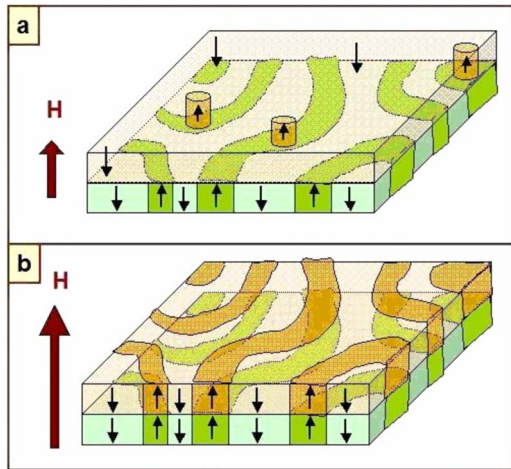


FIG. 4. (Color online) Schematic of the domain reversal in the F/AF junction, with the AF layer on bottom and F layer on top. Magnetic field is applied perpendicularly. The feature in the AF layer represents the magnetic template imprinted into the uncompensated pinned moments. (a) Nucleation point: domains start to nucleate in the F layer at random locations; (b) further in the reversal, beyond the coercive point, the F domain pattern eventually matches the magnetic topology of the AF template. This configuration is unique.

smoothly and mostly reversibly, inducing domain-wall motions without changing the global morphology of the labyrinth pattern. Toward saturation, the magnetic memory eventually vanishes in a fashion symmetrical to the nucleation region. The annihilation of the domains mirrors topologically their nucleation: an increasing degree of randomness drives

the reversal of the last domains, thus progressively leading to the loss of memory.

In conclusion, our results demonstrate that exchange couplings interactions can magnetically pattern a strong mesoscopic magnetic memory in F materials placed in contact with an AF material. This process is enabled by the existence of a “frozen” magnetic template imprinted into the AF layer during the ZFC process. Furthermore, the memory varies strongly along the magnetization loop and can be tuned from zero at the nucleation point to its maximum in the coercive region. These results stimulate further interests, in particular exploring the asymmetrical effects in field-cooled conditions, with variable field strength. More generally, the properties of such systems can be tuned with temperature and structural parameters in order to modify the position and width of the memory plateau. These results are related to and may provide insight into other stripe forming systems such as block copolymers on lithographically or chemically patterned substrates.<sup>33,34</sup> Ultimately one could possibly develop a new branch of memory device technology based on EC induced domain memory. These approaches would facilitate engineering aspects and furthermore help surpassing size limitations, which today are crucial parameters in the data storage industry.

The exchange bias materials were grown at Hitachi Global Storage Technology, San Jose, California, USA. The scattering measurements were performed at the Advanced Light Source. The instrumental development was supported by U.S. Department of Energy (DOE) under Contract No. DE-FG02-90ER45416 and by the U.S. NSF under Grant No. DMR-99-71611. S.K. gratefully acknowledges partial support from the National Science Foundation under Grant No. DMR-0506241.

\*Present address: BYU, Provo, Utah 84602, USA.

†Present address: UCSD, San Diego, California 92093-0401, USA.

<sup>1</sup>G. A. Prinz, *Science* **282**, 1660 (1998).

<sup>2</sup>A. A. Taratorin, M. Xiao, and K. B. Klaassen, *IEEE Trans. Magn.* **40**, 129 (2004).

<sup>3</sup>Y. Zheng *et al.*, *J. Nanosci. Nanotechnol.* **7**(1), 117 (2007).

<sup>4</sup>C. Kittel, *Phys. Rev.* **70**, 965 (1946).

<sup>5</sup>M. Pierce *et al.*, *Phys. Rev. Lett.* **94**, 017202 (2005).

<sup>6</sup>W. H. Meiklejohn, *Phys. Rev.* **102**, 1413 (1956).

<sup>7</sup>J. Nogués and I. K. Schuller, *J. Magn. Magn. Mater.* **192**, 203 (1999).

<sup>8</sup>S. Maat, K. Takano, S. S. P. Parkin, and E. E. Fullerton, *Phys. Rev. Lett.* **87**, 087202 (2001).

<sup>9</sup>D. Mauri *et al.*, *J. Appl. Phys.* **62**, 3047 (1987).

<sup>10</sup>M. Ali *et al.*, *Phys. Rev. B* **68**, 214420 (2003).

<sup>11</sup>O. Hellwig, S. Maat, J. B. Kortright, and E. E. Fullerton, *Phys. Rev. B* **65**, 144418 (2002).

<sup>12</sup>S. Roy *et al.*, *Phys. Rev. Lett.* **95**, 047201 (2005).

<sup>13</sup>H. Ohldag, H. Shi, E. Arenholz, J. Stohr, and D. Lederman, *Phys. Rev. Lett.* **96**, 027203 (2006).

<sup>14</sup>J. Camarero *et al.*, *Appl. Phys. Lett.* **89**, 232507 (2006).

<sup>15</sup>P. Kappenberger *et al.*, *Phys. Rev. Lett.* **91**, 267202 (2003).

<sup>16</sup>A. Scholl *et al.*, *Science* **287**, 1014 (2000).

<sup>17</sup>F. Nolting *et al.*, *Nature (London)* **405**, 767 (2000).

<sup>18</sup>H. Ohldag *et al.*, *Phys. Rev. Lett.* **87**, 247201 (2001).

<sup>19</sup>J. C. Eckert *et al.*, *J. Appl. Phys.* **91**, 8569 (2002).

<sup>20</sup>T. L. Kirk, O. Hellwig, and E. E. Fullerton, *Phys. Rev. B* **65**, 224426 (2002).

<sup>21</sup>I. V. Roshchin *et al.*, *Europhys. Lett.* **71**, 297 (2005).

<sup>22</sup>J. P. Hannon, G. T. Trammell, M. Blume, and D. Gibbs, *Phys. Rev. Lett.* **61**, 1245 (1988).

<sup>23</sup>C. Kao *et al.*, *Phys. Rev. Lett.* **65**, 373 (1990).

<sup>24</sup>J. B. Kortright *et al.*, *J. Magn. Magn. Mater.* **207**, 7 (1999).

<sup>25</sup>K. Chesnel *et al.*, *Phys. Rev. B* **66**, 172404 (2002).

<sup>26</sup>S. Eisebitt *et al.*, *Phys. Rev. B* **68**, 104419 (2003).

<sup>27</sup>K. Chesnel *et al.*, *Phys. Rev. B* **70**, 180402(R) (2004).

<sup>28</sup>S. Eisebitt *et al.*, *Nature (London)* **432**, 885 (2004).

<sup>29</sup>M. S. Pierce *et al.*, *Phys. Rev. Lett.* **90**, 175502 (2003).

<sup>30</sup>K. Chesnel, J. J. Turner, M. Pfeifer, and S. D. Kevan, *Appl. Phys. A: Mater. Sci. Process.* **92**, 431 (2008).

<sup>31</sup>J. B. Kortright *et al.*, *Phys. Rev. B* **64**, 092401 (2001).

<sup>32</sup>M. Pierce *et al.*, *Phys. Rev. B* **75**, 144406 (2007).

<sup>33</sup>S. O. Kim *et al.*, *Nature (London)* **424**, 411 (2003).

<sup>34</sup>E. W. Edwards *et al.*, *Adv. Mater. (Weinheim, Ger.)* **16**, 1315 (2004).